Cerebral Cortex, August 2016;26: 3461–3475

doi:10.1093/cercor/bhw123
Advance Access Publication Date: 12 May 2016
Original Article

ORIGINAL ARTICLE

Corticothalamic Spike Transfer via the L5B-POm Pathway in vivo

Rebecca A. Mease[1,2], Anton Sumser[1], Bert Sakmann[1,3] and Alexander Groh[1,2]

[1]Institute for Neuroscience of the Technische Universität München, 80802 Munich, Germany, [2]Department of Neurosurgery, Klinikum rechts der Isar, Technische Universität München, 81675 Munich, Germany and [3]Max Planck Institute for Neurobiology, 82152 Martinsried, Germany

Address correspondence to Alexander Groh. Email: alexander.groh@gmail.com

Abstract

The cortex connects to the thalamus via extensive corticothalamic (CT) pathways, but their function in vivo is not well understood. We investigated "top-down" signaling from cortex to thalamus via the cortical layer 5B (L5B) to posterior medial nucleus (POm) pathway in the whisker system of the anesthetized mouse. While L5B CT inputs to POm are extremely strong in vitro, ongoing activity of L5 neurons in vivo might tonically depress these inputs and thereby block CT spike transfer. We find robust transfer of spikes from the cortex to the thalamus, mediated by few L5B-POm synapses. However, the gain of this pathway is not constant but instead is controlled by global cortical Up and Down states. We characterized in vivo CT spike transfer by analyzing unitary PSPs and found that a minority of PSPs drove POm spikes when CT gain peaked at the beginning of Up states. CT gain declined sharply during Up states due to frequency-dependent adaptation, resulting in periodic high gain–low gain oscillations. We estimate that POm neurons receive few (2–3) active L5B inputs. Thus, the L5B-POm pathway strongly amplifies the output of a few L5B neurons and locks thalamic POm sub-and suprathreshold activity to cortical L5B spiking.

Key words: adaptation, barrel cortex, corticothalamic feedback, layer 5, POm, somatosensory system, thy-1, VGAT

Introduction

A major input to the mammalian thalamus originates in the cortex from corticothalamic (CT) projection neurons in Layers 5 (L5) and 6 (Hoogland et al. 1987; Sherman 2001; Killackey and Sherman 2003). L5 CT axons target "higher order" thalamic nuclei, where they form large ("giant") synapses with thalamic proximal dendrites (Hoogland et al. 1991; Sherman and Guillery 1996; Veinante, Lavallee, et al. 2000; Killackey and Sherman 2003). Anatomical studies suggest that while these synapses are large, they are also sparse (Bourassa et al. 1995). While counts of L5 CT inputs per POm neuron are lacking, these properties differentiate L5 CT synapses from L6 CT synapses, which are small and numerous (Sherman and Guillery 2006). In brain slices, unitary EPSPs evoked from a single L5B axon can trigger action potentials (APs) in target POm neurons (Groh et al. 2008; Seol and Kuner 2015). This cortical "drive" of POm has been supported by in vivo experiments, as blocking cortical activity showed that POm spiking is contingent upon intact barrel cortex (BC) (Diamond et al. 1992; Groh et al. 2014) and is correlated with cortical Up states (Slezia et al. 2011; Groh et al. 2014). However, the strength and adaptive properties of the CT driver pathway in vivo are unknown. Consequently, the efficacy of spike transfer from the cortex to the thalamus (the CT transfer function) has not been quantified in vivo, and it is unknown which—if any—L5B spike patterns of evoke spikes in POm in the intact brain.

Putative CT spike transfer in vivo is likely to depend strongly on the spiking rate of individual L5B neurons, as L5B-POm synapses are characterized by pronounced, fast depression (Reichova and Sherman 2004; Groh et al. 2008; Seol and Kuner 2015); also

see Li et al. (2003) for similar findings in the visual thalamus. Therefore, the strength of a synapse will depend on the spiking history of the upstream L5B neuron, and—as L5B neurons are the most spontaneously active neurons in the BC (de Kock et al. 2007; Oberlaender et al. 2012)—the transfer function of this pathway should adapt markedly. We hypothesized that frequency-dependent synaptic depression could toggle CT spike transfer between different functional modes (Groh et al. 2008): in keeping with the original definition of "driver synapses" (Sherman and Guillery 2006), we refer here to "driver mode" as a fail-safe transfer mode between pairs of L5B and POm neurons, in which a single presynaptic L5B spike evokes one or more POm spikes. From in vitro measurements, this high gain mode is predicted to only occur for L5B spiking frequencies less than approximately 2 Hz, when the synapses are partially or fully recovered (Groh et al. 2008). In contrast, at higher frequencies, each L5B synapse would be depressed and the pathway would operate in a low gain mode, in which several coincident inputs are integrated to evoke POm spiking.

We address the properties of CT spike transfer in vivo by combining optogenetic manipulations with recordings of L5B and POm sub- and suprathreshold activity in urethane anaesthetized mice. The results show that POm is driven by very sparse CT input most likely of L5B origin. Furthermore, the L5B-POm pathway is not in a constant and stable state of depression, resulting in periodic transitions in CT gain following cortical Up and Down state activity.

Methods

Ethical Approval

All experiments were done according to the guidelines of German animal welfare and were approved by the respective ethical committees.

In Vivo Electrophysiology

Animal preparation and recordings were done with 6- to 8-week-old thy1-ChR2 (line 18) or VGAT-ChR2-EYFP line 8 (Jackson Labs) mice anesthetized with 1% Isofluorane in O_2 (SurgiVet Vaporizer) for the photostimulation experiments or urethane (1.3 µg/g body weight) for simultaneous LFP and juxtacellular recordings. Typically one or 2 experiments (simultaneous L5B/POm recordings, simultaneous L5B/L5B recordings, single L5B or POm recordings) were done per animal. Recordings were made from a total of 56 mice: 22 animals for intracellular POm recordings, 8 animals for simultaneous POm/L5B juxtasomal recordings, 5 animals for simultaneous L5B/L5B juxtasomal recordings, 5 animals for single L5B juxtasomal recordings, 10 animals for single juxtasomal POm recordings, 4 for VGAT POm juxtasomal recordings, and 2 for VGAT cortical juxtasomal recordings.

Depth of anaesthesia was continuously monitored by eyelid reflex, respiration rate, and cortical LFP, and additional urethane (10% of the initial dose) was given when necessary. Respiration rates were usually between 100 and 140 breaths per minute. In the case of isoflurane anaesthesia, concentration of anesthetic was adjusted to reach steady respiration rates around 100 breaths per minute. The skull was exposed, and small craniotomies above BC and POm were made (dura intact). For VGAT photostimulation experiments, the skull above BC was additionally thinned to permit better light penetration into the tissue. The head was stereotaxically aligned (Wimmer et al. 2004) for precise targeting of POm. Target coordinates relative to bregma were (lateral/posterior/depth; in mm) as follows: BC L5B: 3.0/1.1/0.7; POm: 1.25/1.7/2.8-3.0; Motor Cortex: 1.0/-1.0/0.6)

In vivo juxtasomal recordings and biocytin fillings were made as described in Pinault (1996). In brief, 4.5–5.5 MΩ patch pipettes were pulled from borosilicate filamented glass (Hilgenberg, Germany) on a DMZ Universal puller (Zeitz Instruments, Germany). Pipettes were filled with (mM) 135 NaCl, 5.4 KCl, 1.8 $CaCl_2$, 1 $MgCl_2$, and 5 HEPES, pH adjusted to 7.2 with NaOH, with 20 mg/mL biocytin added. Bath solution was identical, except for biocytin. Single units were found by the increase of pipette resistance (2–2.5 times of the initial resistance) measured in voltage clamp mode. A L5B and a POm cell were recorded simultaneously with a ELC-01X amplifier (NPI Electronics, Germany) for POm and a Axoclamp 2B (Molecular Devices, USA) for L5B. Unfiltered and band-pass filtered signals (high pass: 300 Hz, low pass: 9000 Hz) were digitized at 20 kHz with CED Micro 1401 mkII board and acquired using Spike2 software (both CED, Cambridge, UK). Typically, recordings consisted of 1 single unit which was filled at the end of the experiment with biocytin using current pulses (Pinault 1996). Whole-cell single neuron current clamp recordings in POm were done using the "blind patching" approach as described in Margrie et al. (2002). Pipette solution was (in mM) 130 K-gluconate, 10 HEPES, 10 Na-phosphocreatine, 10 Na-gluconate, 4 ATP-Mg^{2+}, 4 NaCl, 0.3 GTP, 0.1 EGTA, 2 mg biocytin, osmolarity approximately 300, and adjusted to pH 7.2 with KOH.

Cell Selection Criteria and Cell Reconstructions

For all L5B recordings, we used a combined photo- and sensory stimulation protocol to validate neurons' locations: L5B neurons were accepted for analysis if 1) photostimuli applied to the cortical surface resulted in rapid, unadapting spiking responses that persisted for the duration of a long photostimulus (3 s), and (2) each neuron responded within 100 ms to whisker stimulation, as the majority of L5B neurons in BC respond to whisker stimulation within this time period (de Kock et al. 2007). This protocol ensured that each putative L5B neuron was both in L5B (photostimulation) and in BC (sensory response). In addition to these physiological parameters, L5B and POm neurons were also filled with biocytin for reconstruction of the locations and morphologies (Fig. 1 and see Supplementary Fig. 1).

After the experiments, mice were euthanized with an overdose of ketamine/xylazine and transcardially perfused with 4% PFA in phosphate-buffered saline. Four hours after fixation, the brain was cut into 100 µm coronal slices and stained for cytochrome C to reveal the VPM/POm border and with DAB to reveal the soma and dendrite of the recorded neuron; both protocols are found in Groh and Krieger (2011).

Six POm neurons and 12 Chr2-L5B neurons were recovered and all showed dendritic parameters (Fig. 1 and see Supplementary Fig. 1 and Tables 1 and 2) consistent with previously published descriptions of these neurons (de Kock et al. 2007; Meyer et al. 2010).

Tracing L5B-ChR2 Projections to POm

For retrograde labelling of POm-projecting cortical neurons, a retrograde tracer (50 nL Cholera toxin B—Alexa 647 conjugate, Invitrogen) was stereotaxically injected into POm of thy1-ChR2 mice as described in detail in Wimmer et al. (2004). After 4 days, the animals were killed with an overdose of urethane (3 µg/g body weight) and perfused transcardially with 4% PFA containing PBS. The brain was removed, and 100 µm coronal sections of the somatosensory cortex and thalamus were obtained

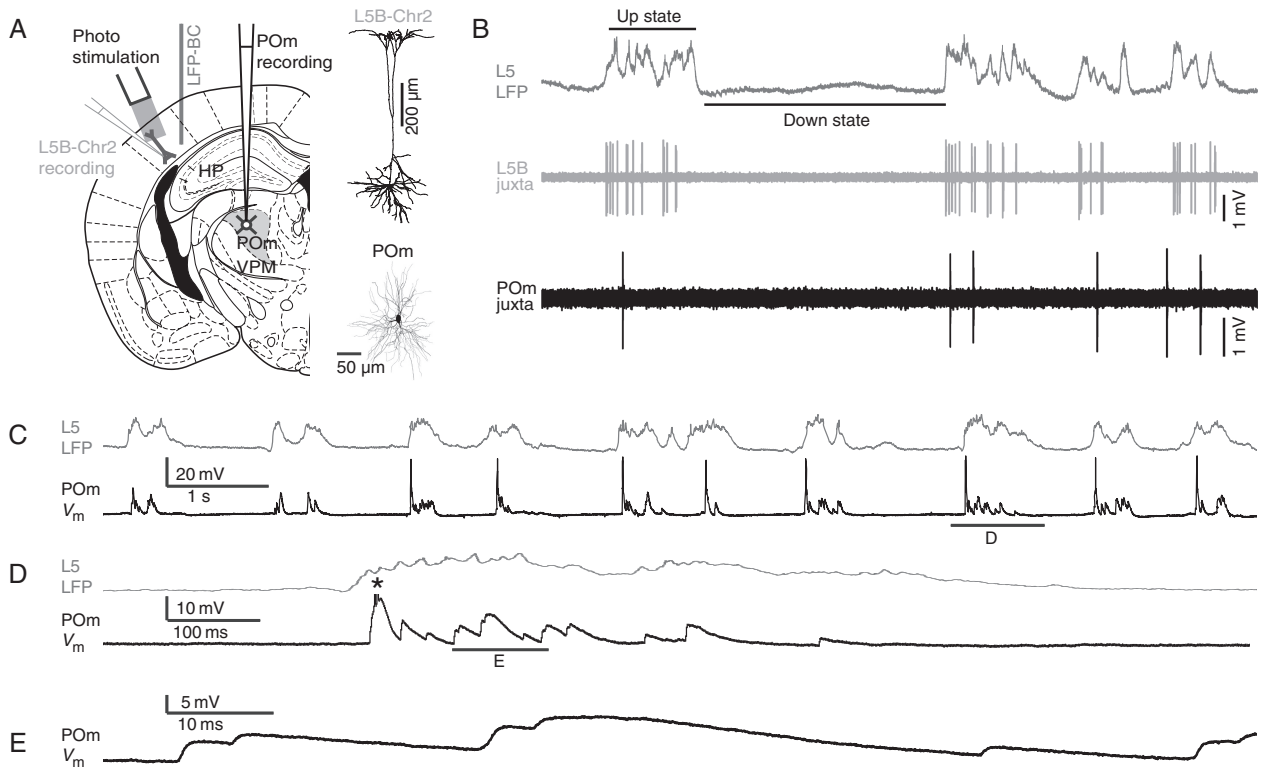

Figure 1. L5B-POm sub- and suprathreshold activity during cortical Up and Down states. (*A*) Left: Experimental setup scheme relative to coronal mouse brain slice, showing BC LFP recording, photostimulation of L5B, and recordings from individual neurons in L5B and POm. Mouse brain slice image modified from Paxinos (2001). Right: representative Neurolucida reconstructions of a L5B-Chr2 neuron (upper) and a POm neuron activated by cortical photostimulation (lower). Additional reconstructions and dendritic morphology parameters are shown in Supplementary Figure 1 and Tables 1 and 2. (*B*) Simultaneous cortical L5 local field potential (LFP, upper) and juxtacellular recordings from L5B (gray, middle) and POm (lower) neurons show L5B and POm spiking during cortical Up states. (*C*) Example of simultaneously recorded cortical L5 LFP and whole-cell patch clamp POm membrane voltage showing cortical Up states and associated POm EPSPs and APs. Resting membrane potential (RMP) = –62 mV. (*D*) Single Up state from *C* at higher time resolution shows a large "driver" EPSP and subsequent AP (truncated) at the start of an Up state and EPSPs of variable size throughout the Up state. (*E*) Short epoch from *D* showing summation of unitary EPSPs at higher time resolution.

on a vibratome (HR2, Sigmann Electronic, Germany). Fluorescence images were acquired using an Olympus FV1000 (Hamburg, Germany) confocal microscope with a ×20 oil objective (NA 0.9).

In Vivo Photostimulation Setup

Stimulation of ChR2 or VGAT neurons was achieved by a custom-built laser setup consisting of a solid state laser (Sapphire, Coherent, Dieburg, Germany) with a wavelength of 488 nm and a maximal output power of 20 mW. The sub-millisecond control of laser pulses was achieved by an ultrafast shutter (Uniblitz, Rochester, NY, USA). The laser beam was focused with a collimator into 1 end of a multimode fiber (Thorlabs, Grünberg, Germany; numerical aperture = 0.48, inner diameter = 125 µm). For ChR2-L5B neuron activation, the maximal output power at the end of the fiber was 1 mW, resulting in a maximal power density of approximately 32 mW/mm^2 on the brain surface. Shutter control was implemented with Spike2 software (CED, Cambridge, UK). The optical fiber was positioned at an angle of approximately 86° (from the horizontal plane) and at a distance of approximately 100 µm to the cortical surface. For each neuron, we recorded an average of 72 ± 58 or 74 ± 47 trials for juxtasomal and intracellular recordings, respectively. For BC VGAT photostimulation, the optical fiber was positioned at the same angle, but at a distance of approximately 2.5 mm to increase the stimulated area to a disc with a diameter of approximately 800 µm above BC. For robust cortical inhibition (see Fig. 3C), we used a 40 Hz series of laser pulses (12.5 ms on, 12.5 ms off) for 1 s with an approximate power density at the pia of 8.4 mW/mm^2, based on the study by Zhao et al. (2011). For each neuron, we recorded an average of 53 ± 18 trials (1 s photostimulation trains).

Cortical LFP Recordings

To monitor cortical state, we acquired L5 local field potentials (LFP) simultaneously with single neuron recordings. Depth-resolved LFPs were recorded with a 16-channel probe (Neuronexus probe model: A1X16-3mm-100-177, Neuronexus, MI, USA). The probe was inserted 1.5 mm from the pia and a Teflon-coated silver wire chlorided at the tip was used as reference in the bath solution above the craniotomy. Signals were amplified and filtered with an extracellular amplifier (EXT-16DX, NPI Elektronics, Tamm, Germany). LFPs were band-pass filtered with 0.01 or 0.1 Hz and 500 Hz corner frequencies and amplified 1000–2000 times. All signals were digitized at 20 kHz with CED Micro 1401 mkII board and acquired using Spike2 software (both CED, Cambridge, UK). Only LFPs recorded at a depth of 750 µm, corresponding to L5B, were used for analysis. Same coordinates as above.

Muscimol Block of BC

To determine the specificity of L5B drive of POm, we blocked barrel cortex (n = 3, Fig. 3) via application of approximately 50 nL of

10 mM muscimol (Sigma Aldrich) injected to L5. Muscimol is a GABA-A receptor agonist and is widely used to locally inhibit neuronal activity in the intact brain (Letzkus et al. 2011; Xu et al. 2012). Under these conditions, muscimol spreads approximately 1 mm along the anterio-posterior axis (Letzkus et al. 2011), thus likely blocking activity in the entire barrel field, and possibly parts of S2 cortex known to form giant synapses with POm neurons as well (Liao et al. 2010). After establishing a whole-cell recording in POm, an injection pipette (Blaubrand) was lowered into BC to a depth of 800 µm below the pia, and the drug was slowly pressure injected into the cortex. Effects on the sub- and suprathreshold activity in POm were seen approximately 5–10 minutes after drug application. We monitored the LFP in motor cortex (MC) while recording from single POm neurons. Despite ongoing Up and Down state activity in MC, spikes and spontaneous large EPSPs in POm successively disappeared 5–10 min after muscimol injection into BC. This treatment was nonreversible in the time course of our experiments.

Data Analysis

Electrophysiology data were acquired using Spike2 software and then exported for analysis in Matlab version 9 (MathWorks, Natick, USA) using custom written software. Spike times were extracted by finding local maxima in the temporal derivative of recorded voltage traces (dV/dt) above a variable threshold (typically 40–50% of maximum dV/dt). Reported values are mean ± standard deviation, unless otherwise noted.

EPSP Extraction

We characterized POm sub- and suprathreshold responses to putative L5B spiking via whole-cell patch clamp recordings ($n = 38$ neurons; >50 000 EPSPs). EPSP amplitude was defined as the EPSP maximum, including all postsynaptic potentials such as low threshold calcium spikes. EPSP times and maxima were extracted by finding crossings in the first derivative of the membrane potential and validated and/or corrected by hand.

Identification of Up States

Up states were selected by hand as large deflections in the LFP. To further standardize transition points across recordings and Up transitions with different rates of change, each individual LFP transition trace was normalized to a height of 1 and the transition point was then set to be the time at which the trace reached 50% of this maximum (see Supplementary Fig. 3). For the display figures, the LFP signal was converted to a dimensionless z-score and then inverted so that positive deflections correspond to "Up states" (Hahn et al. 2006).

Model Construction

EPSP Adaptation

To predict the adaptation state of the L5B-POm pathway, including synaptic and intrinsic factors, we constructed a simple model combining intracellular EPSP measurements and L5B spontaneous spiking statistics. For "single input" POm neurons which 1) showed only one unadapted EPSP amplitude peak and 2) showed high correlation between EPSP amplitudes and inter-EPSP interval (IEI), we normalized all EPSP amplitude by the average unadapted EPSP amplitude. We then plotted normalized EPSP amplitude versus IEI for a subset of single input neurons ($n = 5$). We then fit a double exponential to this curve: $M_{pred}(t) = e^{1-t_{ISI}/\tau_1} + e^{1-t_{ISI}/\tau_2}$, where $\tau_2 = 550$ ms, $\tau_2 = 550$ ms, $t_{ISI} = t - sp_t$, and sp_t is the most recent L5B spike relative to t. Those t_{ISI} >2 s were truncated to 2 s, and we set $M_{pred} = 0$ for $t_{ISI} = 0$, corresponding to a completely depressed synapse. We then used this function to convert experimentally measured L5B spike trains (juxtacellular recordings) into predicted POm EPSP recovery state.

Predicting POm Suprathreshold Events

POm intrinsic properties are highly nonlinear and show significant intrinsic bursting. Our goal here was to predict the timing of POm output relative to cortical input, not the precise spike count dependent on bursting mechanisms. To this end, instead of predicting discrete spikes times, we predicted POm suprathreshold events, in which an "event" could consist of one or more spikes. We first used the predicted POm EPSP recovery state to look up the predicted EPSP amplitude for each L5B spike time (completely recovered amplitude = 1). We then added a scaled version of an unadapted EPSP at each time point corresponding to an input L5B spike. EPSPs were modeled as a difference of exponentials fit to unadapted (IEI >700 ms) isolated (no subsequent EPSPs within a 50 ms window) experimentally measured EPSPs: $EPSP(t) = e^{(1-t/\tau_1)} - e^{(1-t/\tau_2)}$, with $\tau_1 = 12.8$ms and $\tau_2 = 4.8$ms. Time constant fitting was done using a minimum root mean-squared difference between the model EPSP and target normalized voltage trace (normalized to maximum of 1).

Predicted event rates were then found by finding regions of the predicted voltage trace V_{pred} greater than a threshold θ; subsequent regions above θ were combined, corresponding to a minimum interevent interval of 1.5 ms. Unsurprisingly, predicted rates were quite sensitive to θ. For $\theta < 1$, unadapted single EPSPs can drive POm events, whereas for $\theta \geq 1$, either coincident independent L5B inputs or closely spaced EPSPs driven by the same input L5B neuron are required to drive POm output spikes. Predicted event rates were calculated as the number of above threshold regions divided by the total length of the input L5B recording.

Estimating Input Number Based on Correlation

For POm whole cell recordings, we estimated input number based on the correlation coefficient r between POm EPSP amplitude and $\log_{10}$ inter-EPSP interval. This strategy follows from the assumption of strong depression of the L5B-POm synapses (Groh et al. 2008). Single inputs should have a large r with an upper limit set by background noise from synaptic release noise (Groh et al. 2008) and membrane potential fluctuations controlling driving force and availability of the T-channel. It should be noted that this estimate is based in functional rather than anatomical data, that is, active L5B inputs (large and depressing) during spontaneous Up and Down states. The contribution of anatomical L6 inputs is negligible under these experimental conditions, (see Velez-Fort et al. (2014)).

To explore the range of r expected for single and 2 input neurons, we predicted the EPSP size generated in response to our group of simultaneous recorded L5B spike trains ($n = 9$ pairs), and r between IEI and EPSP size calculated for different levels of noise. For single inputs, all spike trains ($n = 18$) were used, and for double inputs, the paired EPSP trains were combined.

To extrapolate the predicted r values for >2 inputs, we generated mock spike trains by drawing from experimentally generated interspike interval distributions from up to 5 independent L5B recordings and then combining the EPSP trains and IEIs as above.

Results

We first measured the cortical input and thalamic output of the L5B-POm pathway by recording simultaneously from L5B and

POm neurons ($n = 12$ pairs) in the juxtacellular configuration (Fig. 1A). These individual L5B and POm neurons in the paired recordings were most likely not connected, because POm is sparsely innervated by L5B (Bourassa et al. 1995). To record from a defined group of L5B neurons in BC, we used the ChR2-expressing thy1 mouse (line 18) that has been used to specifically photostimulate L5 neurons in vivo (Arenkiel et al. 2007; Stroh et al. 2013; Vazquez et al. 2014). This allowed us to confine our cortical data set to a relatively homogenous group of L5B neurons by searching for photo-responsive neurons in L5B during each experiment. Analysis of morphologies showed that ChR2-expressing neurons are thick-tufted L5B neurons (Fig. 1A, top; see Supplementary Fig. 1), consistent with previous descriptions of POm-projecting neurons' morphology (Killackey and Sherman 2003). To confirm that Chr2-positive neurons indeed included POm-projecting neurons, Chr2-positive neurons were labeled by retrograde tracer injections in POm (see Supplementary Fig. 2). Recordings in POm were directed by stereotaxic coordinates, photo-responsiveness to BC L5 stimulation, and confirmed post hoc for a subset of POm recordings ($n = 6$) with recovered dendritic morphologies (Fig. 1A, lower and see Supplementary Table 2). Single L5B ($n = 12$) and POm ($n = 15$) neurons and simultaneously recorded L5B neuron pairs ($n = 9$ pairs) which met the above criteria were included in some analyses. A further set of recordings were done in whole-cell configuration from single POm neurons ($n = 38$) to quantify photo-evoked and spontaneous EPSPs.

L5B and POm Activity During Cortical Up and Down States

Cortical neurons follow spontaneous "Up state" cortical oscillations which occur during anesthesia (Timofeev et al. 1996; Steriade 1997; Constantinople and Bruno 2011). If the L5B-POm pathway supports efficacious CT spike transfer in vivo, then we expect to see correlated cortical and thalamic activity during such Up states. To first determine the relation between cortical Up states, L5B spikes, and POm spikes, we recorded simultaneously from L5B and POm neurons ($n = 12$ cortical/thalamic simultaneous recordings), as well as local field potential (LFP) in L5 of BC to monitor cortical Up states (schematic shown in Fig. 1A). L5B spiking was tightly correlated with cortical Up states. Interestingly, POm spiking was correlated with cortical Up states in a similar but more selective fashion. Both L5B and POm spiking occurred exclusively during Up states and peaked during Up state onsets. However, in contrast to L5B spiking throughout the entirety of each Up state, POm spikes were sparser and nearly always occurred at Down-Up state transitions (Fig. 1B).

To understand the changes in subthreshold activity which might underlie this marked difference between cortical and thalamic spiking, we simultaneously recorded POm membrane potential in whole-cell configuration and cortical LFP from L5 in BC. All POm neurons ($n = 38$) had large EPSPs evoked during spontaneous cortical Up states (Fig. 1C). In contrast, EPSPs were entirely absent during cortical Down states, matching the lack of spiking in L5B (Fig. 1B).

Spontaneous EPSPs in POm as shown in Figure 1E varied widely in amplitude (from 0.5 mV to larger than 20 mV, see Supplementary Fig. 7 for population distribution), with a median amplitude of 4.4 mV (1st quartile 2.6 mV, 3rd quartile: 7.3 mV). Larger EPSPs (>8 mV) often showed stereotyped slow depolarizations consistent with low-threshold calcium spikes (LTS) characteristic of thalamic relay neurons (Jahnsen and Llinas 1984; Landisman and Connors 2007; Groh et al. 2008). Such EPSPs typically triggered one or more APs, and these large AP-triggering EPSPs most often occurred at the beginning of Up states (first event in Fig. 1D). Furthermore, EPSPs showed strong adaptation, meaning that larger EPSPs were often followed at short-time intervals by small amplitude EPSPs (Fig. 1E).

To quantify these initial observations, we next used the Up transitions in the LFP to align and pool spiking, EPSP, and LFP data across recordings (see Methods and see Supplementary Fig. 3). Figure 2 compares the population average activity patterns in L5B and POm during cortical Up states ($n = 16$ L5B and $n = 12$ POm, juxtacellular; $n = 22$, POm intracellular). In all experiments, L5B and POm spiking was tightly coupled to spontaneous Up state transitions (Fig. 2A) and absent during Down states. L5B spike rates (Fig. 2B) were higher than POm spike rates (Fig. 2C) by an approximate factor of 3 (mean spike rates: 1.9 ± 0.8 Hz and 0.63 ± 0.5 Hz, for L5B and POm, respectively, L5B, $n = 16$; POm, $n = 12$; 172–1964 Up states per recording, mean 583 ± 413).

Population EPSP analysis shows that POm EPSPs (Fig. 2D) and L5B spikes (Fig. 2B) follow a similar progression through the Up state: peaking at the beginning of the Up state and slowly declining for the duration, consistent with POm activity being dominated by large L5B EPSPs during spontaneous Up states. Mean spontaneous EPSP rate was 3.8 ± 2.1 Hz ($n = 38$), and EPSP amplitudes (Fig. 2E) peaked in the beginning and declined by approximately 40% throughout the Up state. The time course of this adaptation suggests that the strength of L5B-POm synapses is periodically modulated by cortical Up and Down states and the associated changes in L5B spiking, with the result that CT spike transfer is most effective at Up state transitions when the L5B-POm synapse is maximally recovered after L5B inactivity during preceding Down states.

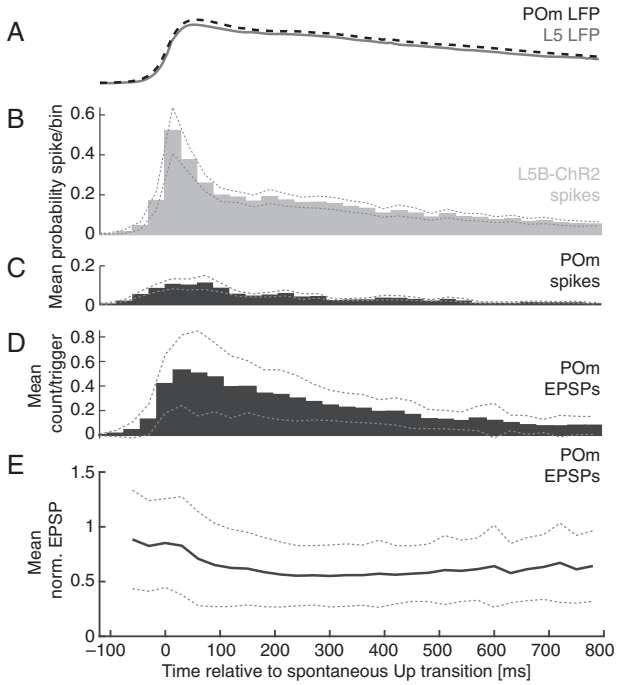

Figure 2. Summary of L5B-POm sub- and suprathreshold activity triggered on Up state transitions. (*A*) Mean LFP (from recordings in L5B in gray and POm in black dashed line) and histograms of (*B*) L5B (gray, $n = 16$) and (*C*) POm (black, $n = 12$) spikes triggered on spontaneous Up state transitions. Dotted lines show standard error of mean. See Methods and Supplementary Figure 3 for extraction of Up transitions. (*D*) Population mean spontaneous POm EPSP arrival histogram triggered on spontaneous Up states ($n = 22$ POm neurons). Dotted lines show SD. (*E*) Population mean normalized EPSP amplitudes ± SD for data in *D*.

Previous in vitro work suggested that POm neurons might be driven by single L5B spikes from single L5B neurons or, when the L5B-POm synapses are depressed, integrate 2 or more L5B spikes (Groh et al. 2008). Here, in the in vivo intracellular data set, we categorized POm APs by the number of EPSPs in the preceding 30 ms window. A population median of 45% of all APs (1st and 3rd quartiles, 21% and 0.61%, respectively) was driven by single EPSP (median amplitude = 8.7 mV; 1st and 3rd quartiles, 6.4 and 14.8 mV, respectively) and the remaining 55% by 2 or more EPSPs (median amplitude 5.0 mV, 1st and 3rd quartiles, 3.2 and 7.4 mV, respectively). Single EPSPs that triggered APs were nearly twice the amplitude of integrated EPSPs ($P < 0.05$, rank sum). This analysis suggests that, regardless of the number of anatomical L5B inputs, POm spikes can signal either the integration of 2 or more L5B spikes, or the occurrence of single L5B spikes, and that EPSP adaptation transitions L5B-POm spike transfer between the 2 modes.

EPSPs and Spiking in POm Depend on Cortical Input

The tight coupling of L5B spikes and POm EPSPs (Figs 1 and 2) suggests a causal relation between L5B in BC and POm activity. To test this causality, we inhibited BC pharmacologically and optogenetically. Spontaneous large EPSPs and APs in POm were abolished by muscimol injection into BC, with EPSP rates declining from approximately 3 to 0 Hz (Fig. 3A,B). While muscimol injection abolished Up states in BC (see Supplementary Fig. 4), Up states persisted in motor cortex (MC) (Fig. 3A, middle), suggesting that the drug remained relatively restricted to somatosensory cortex. Similarly, inhibiting BC in a more spatially and temporally specific manner via cell-type-specific photostimulation of inhibitory VGAT interneurons (Fig. 3C) (Zhao et al. 2011) immediately and reversibly abolished spontaneous POm spiking (Fig. 3D,E). These data show that in the anesthetized animal, cortical input —most likely of BC origin—is required for POm spiking. These data are in agreement with previous, less region-specific manipulations such as cortical cooling (Diamond et al. 1992) and cortical spreading depression (Groh et al. 2014).

EPSPs in POm Are Evoked by Photostimulation of L5B Neurons in BC

To directly confirm the L5B origin of large EPSPs in POm (Reichova and Sherman 2004; Groh et al. 2008), we photostimulated L5 neurons in BC and recorded subthreshold responses in POm, as before (Groh et al. 2014). Photostimulation with short (5 ms, <32 mW/mm^2) laser pulses applied to the surface of BC evoked sharp deflections in the L5 LFP and short latency, high probability spikes in L5B and POm neurons (Fig. 4A,B). To measure EPSP latencies and test whether EPSPs were unitary, we made whole-cell recordings of photo-evoked responses in POm (Fig. 4C). Under minimal stimulation conditions with low intensities, we

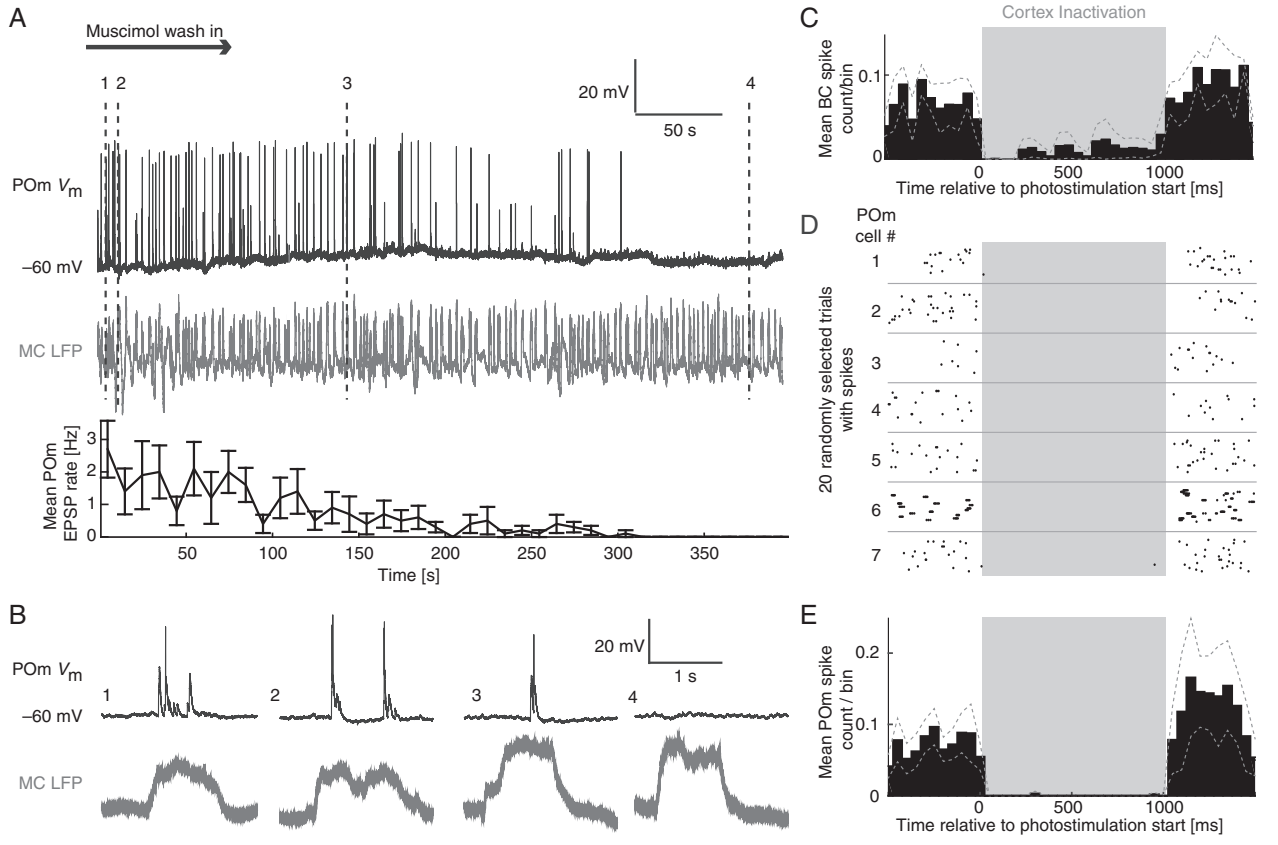

Figure 3. POm sub- and suprathreshold activities are suppressed by cortical inhibition. (*A*) Upper panel: POm whole-cell recording, (RMP = –60 mV), showing spiking and EPSPs during BC muscimol wash in. Middle panel: simultaneous LFP recorded in motor cortex maintained Up and Down states. Lower panel: Mean EPSP rate as a function of time; each data point is the average EPSP rate for ten 1 s bins, ± SEM. (*B*) Zoom of traces marked in A to show detail of motor cortex UDS and POm sub- and suprathreshold responses. (*C*) Population mean PSTH ($n = 4$) of infragranular (depth >730 µm from pia) BC neurons' spontaneous activity during cortex inactivation (VGAT photostimulation). Spontaneous rates decreased from 1.7 ± 0.5 to 0.21 ± 0.18 Hz (mean ± SEM) during cortex inactivation (VGAT photostimulation). (*D*) Example spike rasters from POm juxtacellular recordings ($n = 7$) aligned to cortex inactivation (VGAT photostimulation). (*E*) Population mean PSTH ($n = 7$) of POm cells shown in (*D*) with dashed lines showing SEM. Spontaneous rates decreased from 1.8 ± 0.4 to 0.03 ± 0.01 Hz (mean ± SE) during cortex inactivation (VGAT photostimulation).

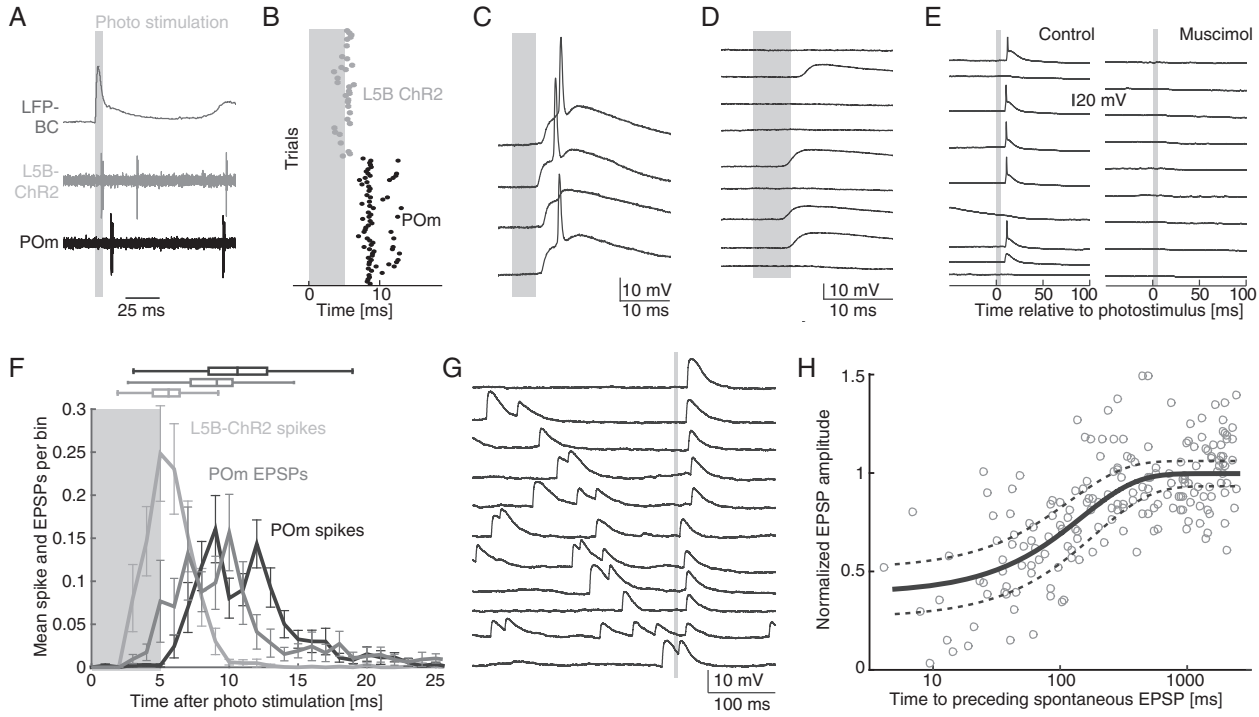

Figure 4. Photostimulation of L5B-POm pathway. (*A*) Example dual L5B/POm juxtacellular recording with photostimulation (gray bar) shows that both L5B and POm neurons sequentially respond to photostimulation. Simultaneously recorded cortical L5 LFP recording shown as the top trace. (*B*) Raster of spike responses to photostimulation for dual L5B and POm recording in A shows timing of first spikes: L5B approximately 5 ms and POm approximately 8 ms. (*C*) POm whole-cell responses to photostimulation: large EPSPs and APs and AP failure trials. RMP = −63 mV. (*D*) Same as C under minimal photostimulation conditions shows EPSP failures and large unitary EPSPs with amplitudes of >5 mV. (*E*) POm whole-cell recording of responses to L5B photostimulation before (left) and after (right) injection of muscimol into BC. RMP = −65 mV. (*F*) Population summary of response delays after photostimulation. Photo-evoked L5B (light gray) and POm (black) spikes. Median and 1st (1st quartile) and 3rd (3rd quartile) quartile spike latencies: L5B = 5.6 ms (1st quartile: 4.45 ms, 3rd quartile: 6.35 ms, $n = 1756$ spikes, 31 L5B neurons) and POm = 10.6 ms (1st quartile: 8.5 ms, 3rd quartile:12.75 ms, $n = 1367$ spikes, 38 POm neurons). The average delay from L5B spikes to POm spikes was 5 ms. Photo-evoked POm EPSP delays (dark gray) were 9.1 ms (1st quartile: 7.2 ms, 3rd quartile: 10.2 ms, $n = 1239$ EPSPs, 16 POm neurons). Thus, the delay between L5B spikes to POm EPSPs is 3.5 ms, ruling out polysynaptic activation. All medians were significantly different (rank-sum test). (*G*) Traces of evoked EPSPs preceded by spontaneous EPSPs in an example POm whole-cell recording, RMP = −62 mV; gray line shows time of photostimulation. Traces sorted by increasing interval between spontaneous and evoked EPSPs, showing that amplitudes of evoked EPSPs depend on the time to previous spontaneous EPSPs. (*H*) Photo-evoked EPSP amplitude versus $\log_{10}$ time to preceding spontaneous EPSP, population data ($n = 7$). To pool data across cells, photo-evoked EPSP amplitudes were normalized by mean isolated EPSP amplitudes per cell (no spontaneous EPSPs within 500 ms of light stimulus). Exponential fit (solid line) and error of fit (dashed line).

observed failure trials with no responses interspersed with successful trials consisting of large, unitary EPSPs (Fig. 4*D*). In addition, these EPSPs were blocked by muscimol injections into BC (Fig. 4*E*), confirming that these events were driven by cortical input.

Additional cortical input to POm originates in cortical layer 6 (L6) (Hoogland et al. 1987; Bourassa et al. 1995; Killackey and Sherman 2003). However, our L5B photostimulation protocol did not activate L6 neurons, which do not express ChR2 in the thy-1 mouse line (Arenkiel et al. 2007), and secondary activation of L6 via L5 cortico–cortico pathways was only seen for laser strengths approximately an order of magnitude greater than that we used for our photostimulation experiments (see Supplementary Fig. 5). Additionally, both spontaneous and photo-evoked POm EPSPs are incompatible with L6-evoked inputs: L6 inputs to the thalamus evoke EPSPs that 1) are about an order of magnitude smaller than EPSPs evoked by L5B inputs, 2) scale linearly with stimulation strength, and 3) are accompanied by simultaneous hyperpolarization (Reichova and Sherman 2004; Landisman and Connors 2007; Mease et al. 2014).

Finally, analysis of the response delays along the L5B-POm pathway strongly suggested monosynaptic activation (Fig. 4*F*). Photo-evoked L5B spikes occurred with a median delay of 5.6 ms (1st quartile: 4.45 ms, 3rd quartile: 6.35 ms, $n = 1756$ spikes, 31 L5B neurons), comparable to an earlier report by Arenkiel et al. (2007). Median photo-evoked EPSP onsets were 9.1 ms (1st quartile: 7.2 ms, 3rd quartile: 10.2 ms, $n = 1239$ EPSPs, $n = 16$ POm neurons) and median POm spike delays were 10.6 ms (1st quartile: 8.5 ms, 3rd quartile: 12.75 ms, $n = 1367$ spikes, $n = 38$ POm neurons) after photostimulus onset (Fig. 4*F*). In summary, the delays between photo-evoked L5B spikes and POm EPSPs or spikes were 3.5 and 5 ms, respectively, matching predictions from axon velocity measurements of this pathway (Kelly et al. 2001) and ruling out polysynaptic activation.

Interaction Between Evoked and Spontaneous POm Activity

These data strongly suggest that photo-evoked EPSPs in POm result from direct input from L5B (Fig. 4*C*,*D*,*F*). We reasoned that if both spontaneous and photo-evoked POm EPSPs and spikes are triggered by the same L5B inputs, spontaneous and evoked events measured in a single POm neuron should show statistical interaction due to synaptic depression (Reichova and Sherman 2004; Groh et al. 2008).

Spontaneous EPSPs did indeed affect subsequent photo-evoked EPSPs, in that the amplitudes of photo-evoked EPSPs decreased with the occurrence of spontaneous EPSPs

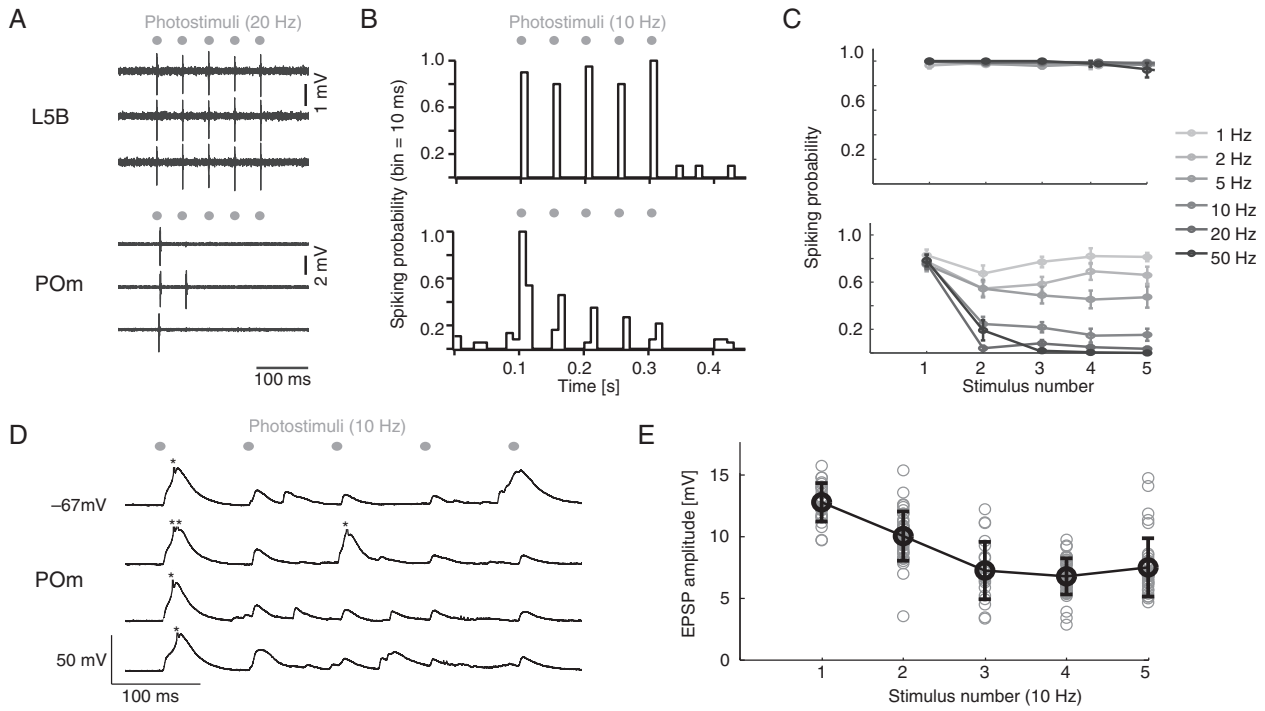

Figure 5. Photostimulation of L5B elicits frequency-dependent CT adaptation in vivo. (*A*) Example traces of juxtacellular recordings in a L5B neuron (upper) and a POm neuron (lower) photostimulated at 20 Hz. (*B*) PSTHs for juxtacellularly recorded spikes for a L5B neuron (upper) and a POm neuron (lower) photostimulated at 10 Hz. (*C*) Average spiking probabilities of 12 L5B-Chr2 (upper) and 15 POm neurons (lower) for photostimulus trains applied at different frequencies (1, 2, 5, 10, 20, 50 Hz). (*D*) Example traces of membrane voltage of a POm neuron during L5B photostimulation at 10 Hz, showing reduction of EPSP amplitudes over the stimulation train. RMP = –67 mV. Action potentials are truncated (*). (*E*) Scatter plot of EPSP amplitudes in POm in response to L5B stimulation at 10 Hz in a POm neuron. Single trials in gray, mean amplitudes in black. Error bars show SD. (*A–E*) As with single photostimulation pulses, individual pulses in the frequency trains were 5 ms long.

preceding the photostimulus (Fig. 4*G*). Consistent with frequency-
dependent depression of the L5B-POm pathway (Li et al. 2003; Reichova and Sherman 2004; Groh et al. 2008), population analysis of photo-evoked EPSPs showed that EPSP amplitude increased with time to preceding spontaneous EPSPs (Fig. 4*H*), showing significant interaction within a window of 500 ms. This timescale of adaptation matches that described previously in vitro (Groh et al. 2008). Similarly, on the suprathreshold level, spontaneous POm spiking decreased the probability of spiking responses to subsequent photostimuli (see Supplementary Fig. 6). Thus, in agreement with previous anatomical and functional data from the L5B-POm pathway (Hoogland et al. 1987; Diamond et al. 1992; Reichova and Sherman 2004; Groh et al. 2008), these in vivo interactions of spontaneous and evoked supra- and subthreshold activity suggest that both inputs originate in L5B of the BC.

Frequency-Dependent Adaptation of L5B-POm Pathway in vivo

The spontaneous and photo-evoked data show evidence of adaptation which should be strongly frequency dependent due to depression of the L5B-POm synapse (Reichova and Sherman 2004; Groh et al. 2008). We directly tested the in vivo frequency dependence of CT spike transmission with repeated (5) brief (5 ms) photostimuli presented at frequencies from 2 to 50 Hz (Fig. 5). L5B neurons spiked with high probability across the entire frequency range (Fig. 5*A–C*, upper panels), while POm spike responses decreased with stimulation frequency (Fig. 5*A–C*, lower panels). Thus, the efficacy of CT spike transfer strongly adapts according to the frequency of L5B input, with the most pronounced CT gain adaptation occurring for frequencies of 10 Hz and more (Fig. 5*C*). Examining subthreshold adaptation in whole-cell POm recordings (Fig. 5*D,E*) shows that photo-evoked EPSPs adapt significantly to high frequency stimulation, although with occasional recovery likely due to T-type calcium channel deinactivation. In sum, this rapid gain adaptation allows the L5B-POm pathway to operate dynamically according to the spiking patterns of L5B neurons, as in the spontaneous Up state data (Fig. 2).

EPSP Adaptation Across the L5B-POm Pathway

The variability in EPSP amplitudes in individual POm recordings was high, spanning almost an order of magnitude (see Supplementary Fig. 7). While some degree of variability was due to varying membrane potential at EPSP onset (see Supplementary Fig. 7*D*), we reasoned that a large amount of amplitude variation was due to different degrees of depression in L5B-POm synapses induced by variable intervals between spontaneous input L5B spikes. In a given POm recording, intervals between input L5B spikes can be inferred from inter-EPSP intervals (IEIs) in the recorded recipient POm neuron. Assuming strong depression at the L5B-POm synapse (Groh et al. 2008), in a POm neuron receiving input from a single L5B neuron, EPSP size should increase with long IEIs that allow the synapse to recover from depression. We found that a subset of neurons indeed matched this expectation (Fig. 6*A*). These neurons could be identified by a characteristically strong correlation between EPSP amplitude and IEI (Fig. 6*B*), whereas the remainder of recordings showed a weaker correlation (Fig. 6*C,D*).

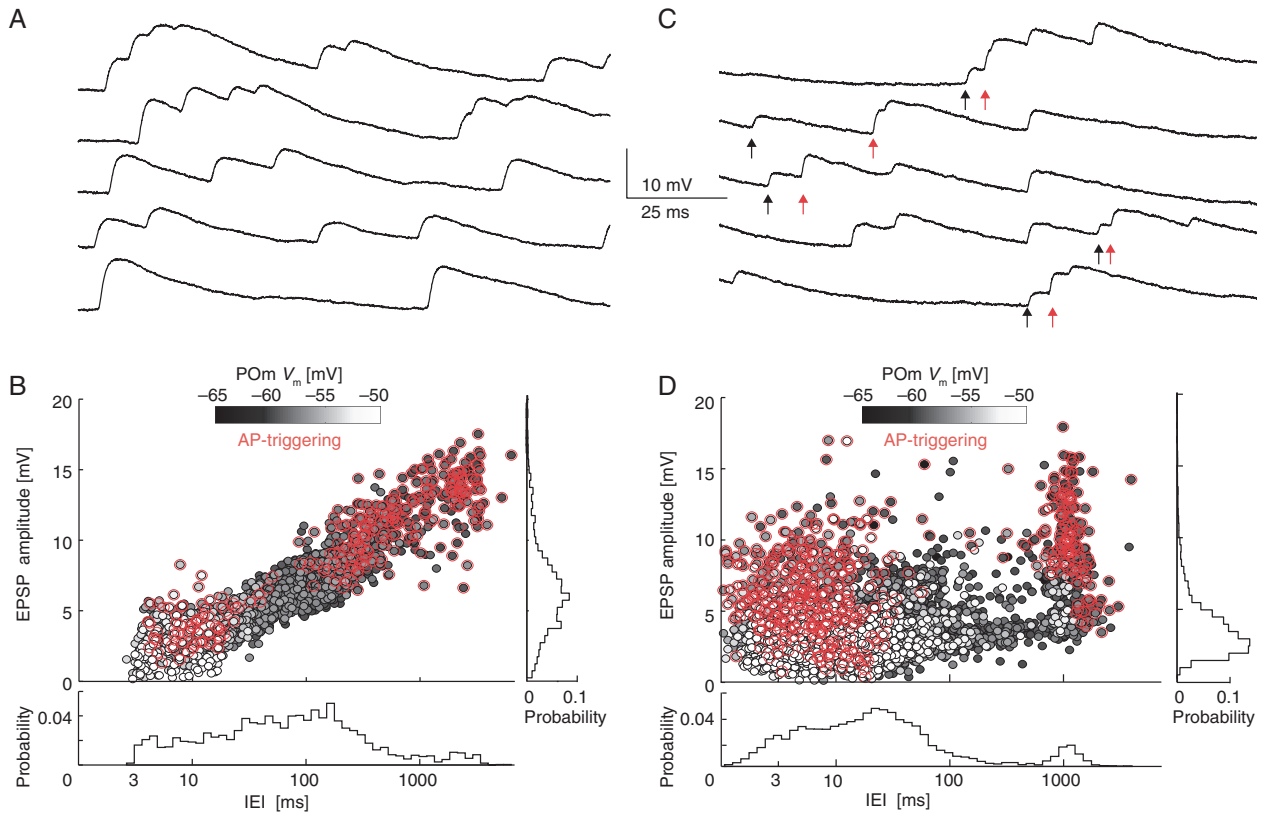

Figure 6. Adaptation of spontaneous POm EPSPs in "single" and "multiple" input neurons distinguished by correlation between EPSP amplitude and IEI. (*A*) Example spontaneous EPSPs; for this POm neuron, large EPSPs are always followed by smaller EPSPs at short IEIs, suggesting a single L5B input. RMP = −65 mV. (*B*) EPSP amplitude versus $\log_{10}$ IEI of the neuron shown in (*A*) displays strong correlation, $r = 0.89$, $n = 2031$ EPSPs. Marginal distribution to right shows EPSP amplitudes (first quartile, median, third quartile 4.3, 6.1, 8.1 mV). Marginal distribution of IEIs shown below (first quartile, median, third quartile: 21.3, 69.6, 177.5 ms). Grayscale shading of markers indicates membrane potential at event onset (lighter points are more depolarized). Red overlay highlights EPSPs that triggered action potentials. (*C*) Example traces showing multiple L5B inputs to POm. Arrows indicate large (unadapted) EPSPs (red) following smaller EPSPs (black). For this recording, approximately 45% of all recorded EPSPs were larger than would be predicted for adaptation of a single input. RMP = −67 mV. (*D*) EPSP amplitude versus $\log_{10}$ inter-EPSP intervals (IEI) during cortical Up state show poor correlation, $r = 0.349$, $n = 6549$ EPSPs in the neuron shown in (*C*). Marginal distribution of EPSP amplitudes shown to right (first quartile, median, third quartile: 2.2, 3.1, 4.8 mV); marginal distribution of IEIs shown below (first quartile, median, third quartile: 6.8, 18.8, 43.0 ms). Color conventions as in *B*.

We used this variation in adaptation to discriminate between POm neurons receiving different number of L5B inputs by calculating the correlation coefficient *r* between EPSP amplitude and $\log_{10}$IEI for each neuron. The logic is as follows: for a neuron with only one depressing input, EPSP amplitude should always be perfectly predicted by IEI (high *r*); in contrast, additional independent inputs will intersperse nonadapted EPSPs in the EPSP train and decrease *r*. A similar approach was used by Deschenes et al. (2003) to estimate the number of lemniscal inputs to VPM neurons.

Categorizing POm Neurons by Putative L5B Input Count

We used *r* to assign each POm neuron a category according to putative independent L5B input count. Nearly half (18/38) of the POm neurons showed a markedly simple relationship between EPSP amplitude and IEI: large EPSPs were always preceded by long IEIs, and small EPSPs occurred exclusively after short preceding IEIs (Fig. 6A). This reliable adaptation led to a high *r* between spontaneous IEI and EPSP amplitude (Fig. 6*B*). We categorized such neurons ($r > 0.6$) as "single input" neurons, as this high correlation could only arise if all observed EPSPs were driven by the same source L5B neuron (or if multiple L5B were always perfectly synchronized—a very unlikely situation). Single input recordings also had a clearly defined minimum IEI (~3 ms see Fig. 6*B* lower histogram). We interpret this minimum IEI as corresponding to the highest spiking rate of the single active input L5B neuron.

The remainder (20/38) of cells showed relatively weaker correlation ($r < 0.6$) between EPSP amplitude and preceding IEI (Fig. 6*C*,*D*) and were termed "multiple input" recordings. These recordings showed mixes of small and large EPSPs not unambiguously predicted by IEI (Fig. 6*C*, arrows), suggesting 2 or more active L5B inputs. In contrast to single input neurons, multiple input neurons showed a continuous distribution of IEIs approaching 0 ms (Fig. 6*D*, lower histogram), further suggesting that the EPSPs arose from multiple independent L5B inputs.

Predicting the CT Spike Transfer Function and the Number of Active L5B Inputs per POm Neuron

The data presented so far suggest that CT gain in the L5B–POm pathway is a function of synaptic depression. In the following, we use experimental data to construct a simple model to predict POm spiking in response to L5B spiking patterns.

The observation of "single input" POm neurons allowed us to quantify POm EPSP amplitude as a function of IEI and thereby the

in vivo adaptation of L5B-POm inputs. We used this adaptation curve (see Supplementary Fig. 8A) to predict POm EPSP amplitudes (unitless, with maximum of 1, corresponding to a completely recovered input) for L5B spikes recorded during Up states (Fig. 7A). Figure 7B shows the recovery of EPSP amplitudes towards 1 between L5B spikes, and the subsequent "adaptation" to 0 at the time of each L5B spike. The time course of predicted EPSP amplitude (Fig. 7C, lower)—the effective CT subthreshold gain—closely followed the in vivo Up state in the LFP (Fig. 7C, upper), supporting our experimental finding that CT gain is controlled by L5B spiking history.

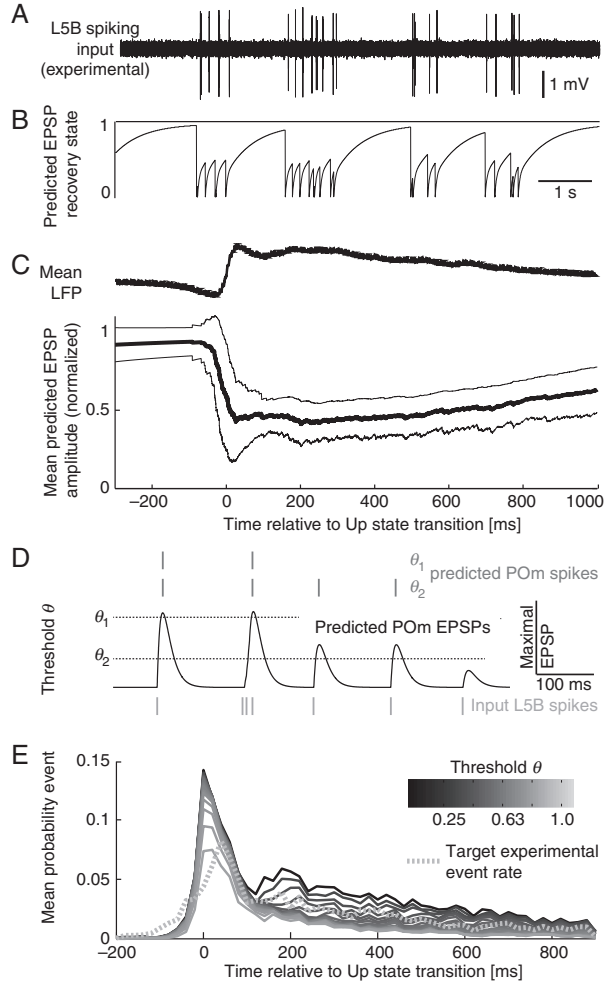

Figure 7. Simple predictive model for EPSP adaptation state. (*A*) Experimental L5B juxtacellular spikes during Up states taken as input to the model. (*B*) L5B spike history is translated into EPSP recovery state as a function of time by using the adaptation curve shown in Supplementary Figure 8*A* as a lookup table. (*C*) Mean cortical Up state transitions (upper) used as a reference signal for L5B-POm adaptation state. Mean ± SD adaptation state (lower, bold line and thin lines, respectively) triggered on cortical Up state transitions shows that recovery (=CT gain) of the L5B-POm pathway follows a similar course as cortical Up states. (*D*) Predicted POm EPSPs for a juxtacellular recording of L5B spontaneous spiking. Threshold lines indicate the degree of depolarization over which POm spiking is expected. L5B spikes preceded by a long silent interval trigger EPSPs exceeding spike threshold. (*E*) Predicted population POm spike event rates in response to experimental spike patterns of single L5B neurons during Up states. Population average predicted event probability shown over a range of thresholds (gray scale), triggered on Up state transitions. For comparison, experimentally measured mean POm event rate is overlaid (dashed line).

By using instantaneous EPSP adaptation state controlled by L5B spikes (Fig. 7*B*) as a multiplier for a template POm EPSP sampled from whole-cell recordings (see Methods), we could create predicted EPSP trains in response to experimentally measured L5B spike trains (Fig. 7*D*). Using these simulated EPSP trains, we next predicted POm spiking events to input L5B spiking patterns using a variable threshold θ (dashed lines in Fig. 7*D*). The time course of predicted POm spiking event times during Up states was similar to the observed experimental time course (Fig. 7*E*). Furthermore, predicted POm event rates best matched experimental values (~0.5 Hz) for θ corresponding to EPSPs recovered to 60–80% of maximal amplitude (see Supplementary Fig. 8). These predictions are consistent with a situation in which POm spiking during Up states are driven largely by L5B inputs, with temporal dynamics determined by subthreshold EPSP adaptation.

Estimating L5B Functional Convergence in POm

We next used 2 approaches—simulated EPSP trains and ratios of experimentally measured spike and EPSP rates—to estimate the number of L5B inputs converging on single POm neurons.

The logic of the simulated EPSP approach is to calculate *r* values from model-generated EPSP trains in response to defined numbers of L5B input patterns and compare those with the experimental *r* values from our intracellular data set (Fig. 8*A*). *r* values depend on 1) the number of L5B inputs, with *r* decreasing as the number of active inputs increase and 2) the variation in experimentally measured EPSP amplitude at a given IEI (EPSP noise). To first test this approach, we made simultaneous recordings from pairs of L5B neurons ($n = 9$ pairs) and used these spike patterns to generate simulated EPSP trains. We then calculated *r* values from simulated EPSP trains (see Supplementary Fig. 8*B*) from either 1) single L5B neurons ($n = 18$, Fig. 8*B* black) or 2) from pairs of L5B neurons ($n = 9$, Fig. 8*B*, red).

Predicted *r* for single inputs was greater than that predicted for 2 simultaneous inputs, and *r* decreased with the addition of EPSP noise. At noise levels matching those observed in vivo (~15%), predicted *r* for single inputs was in agreement with the maximal *r* measured in experimental data ($r = 0.87$). For 2 L5B inputs, *r* values were very similar to the median of all experimental *r* values, suggesting that the number of active L5B inputs per POm neuron may be around 2. Furthermore, these results support the validity of using *r* to discriminate between POm neurons with single and multiple inputs.

To test for 3 or more L5B inputs, we created artificial L5B spike trains by bootstrap resampling (Efron and Tibshirani (1991), 500 repetitions) from in vivo L5B spike trains to simulate POm EPSP trains for up to 5 independent L5B inputs. As in the paired protocol, *r* decreased with input count and EPSP noise, and up to 4 inputs were discriminable by *r* value (Fig. 8*C*). The experimental median *r* value was between the simulated *r* values from 2 and 3 L5B inputs, suggesting that POm neurons receive between 2 and 3 active L5B inputs. Comparing the simulated *r* values from increasing numbers of L5B inputs to experimentally measured *r* values allows an estimation of the number of active L5B inputs converging onto individual POm neurons (Fig. 8*D*). We found that roughly half of the cells in our sample received 1–2 inputs, and the remaining, 3 or more inputs, resulting in a mean of 2.5 L5B inputs per POm neuron.

Next, we independently estimated L5B-POm convergence by comparing L5B spike and POm EPSP rates (Fig. 8*D*). From 500 bootstrap resamples of L5B spike trains, we calculate that 1, 2, 3, 4, and 5 L5B inputs should result in mean POm EPSP rates of 1.5 ± 0.8, 3.4 ± 1.2, 4.7 ± 1.2, 6.4 ± 1.6, and 8.3 ± 1.6 Hz, respectively. Thus,

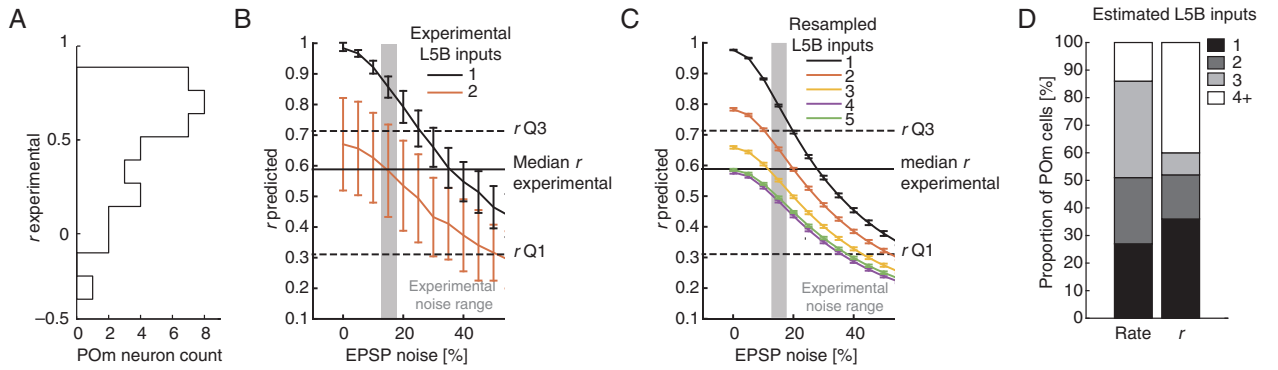

Figure 8. Estimating L5B to POm convergence. (*A*) Distribution of correlation coefficients between EPSP amplitude and $\log_{10}$IEI for 38 POm neurons (median: $r = 0.59$, 1st quartile: $r = 0.32$, 3rd quartile: $r = 0.72$, $n = 38$). (*B*) Mean ± SD of the correlation coefficient (r) between $\log_{10}$IEI and predicted EPSP amplitude for single (black) and paired experimental (red) L5B spikes, as a function of EPSP amplitude noise (additive Gaussian noise). Vertical gray bars and horizontal lines show experimentally measured noise level and correlation coefficient, respectively (median, first and third quartiles). POm EPSP noise was determined from unadapted EPSPs from "single input" whole-cell recordings: median noise value at given IEIs was 15% (1st quartile: 13%, 3rd quartile: 18%). (*C*) As in (*B*), but calculated for 1–5 artificial L5B spike trains resampled from interspike intervals (ISIs) of experimentally recorded L5B neurons. Each marker shows the mean predicted r, calculated for random combinations of 1–5 recorded neurons, 20 000 ISI draws. (*D*) Estimated distributions of L5B input count on POm neurons predicted by 2 different independent calculations: ratios between L5B spike and POm EPSP rates (rate) or correlation coefficient r between predicted EPSP amplitudes and IEI.

the mean experimental spontaneous POm EPSP rate of 3.8 ± 2.1 Hz ($n = 38$) measured here suggests that POm neurons on average receive input from 2–3 L5B neurons, in agreement with the estimation method using r. In summary, these estimates support a view in which L5B-POm functional convergence is sparse under conditions of slow cortical oscillations, with approximately 2.5 L5B neurons dominating the activity of postsynaptic targets in POm.

Discussion

The role of POm in the whisker system is not known, and recent independent demonstrations that whisker self-motion is poorly encoded in POm (Moore et al. 2015; Urbain et al. 2015) make POm even more puzzling. The absence of simple sensory modulation of POm activity highlights the possible importance of extra sensory inputs to higher order thalamus. Here, we investigate the input from cortical L5B to POm and ask how efficiently spikes can be transferred via this pathway in vivo. We determine the relation between the cortical activity patterns and CT gain and predict the convergence of L5B inputs on individual POm neurons.

We find that during low-frequency cortical oscillations typical for anaesthetized, sleeping, and "quietly wakeful" animals (Poulet and Petersen 2008; Constantinople and Bruno 2011; Vyazovskiy et al. 2011; Reimer et al. 2014), the POm membrane potential is characterized by the occurrence of large unitary ("giant") EPSPs (Fig. 1C–E). In combination with a set of control experiments incorporating cell-type-specific photostimulation (Figs 3 and 4), pharmacology (Fig. 3), and EPSP analysis, these data provide evidence that during the cortical Up state oscillations occurring in vivo, spiking in POm is mainly driven by L5B.

Specificity of BC L5B Synaptic Input to POm

Previous anatomical (Hoogland et al. 1987; Bourassa et al. 1995; Killackey and Sherman 2003), synaptic physiology (Reichova and Sherman 2004; Groh et al. 2008), and in vivo (Diamond et al. 1992; Groh et al. 2014) studies demonstrated large ("giant") EPSPs in POm of BC-L5B origin. In addition to L5B neurons in BC, other sources may contribute to the POm activity investigated here: somatosensory cortex 2 (S2, Liao et al. (2010)), motor cortex (Hooks et al. 2013), and SpVi (Chiaia et al. 1991; Veinante, Jacquin, et al. 2000). These inputs are well-established on anatomical grounds, but physiological data about their contribution to POm activity during Up and Down state activity are missing. Here, we provide evidence that in the absence of sensory stimulation, POm activity is dominated by L5B neurons in BC.

Firstly, optogenetic control of L5B activity in BC evoked (Fig. 4) or eliminated (Fig. 3) large, unitary EPSPs in POm. Photo-evoked EPSPs had response latencies incompatible with polysynaptic activation (Fig. 4). Furthermore, L5B spikes in BC and POm EPSPs show very similar patterns during Up and Down states (Fig. 2).

Secondly, SpVi neurons in the brainstem also make large synapses in POm (Chiaia et al. 1991; Veinante, Jacquin, et al. 2000; Lavallee et al. 2005), but these inputs exhibit almost no background firing during anesthesia (Furuta et al. 2010; Groh et al. 2014) and are thus unlikely to be the origin of cortical Up state evoked activity in POm. The photo-evoked EPSPs had average latencies of approximately 3.5 ms and are thus unlikely be triggered via multisynaptic activation of SpVi, which is activated by the cortex with much longer latencies of approximately 10 ms (Furuta et al. 2010).

Finally, L5B in S2 (Liao et al. 2010) and deep layers of motor cortex (Hooks et al. 2013) are additional sources of CT synapses in POm and may potentially contribute to the activity we describe here. While the optogenetic and pharmacological suppression of BC was relatively region specific, suggesting BC as the dominant input during Up and Down states (Fig. 3), better spatial control of cortical activity is needed to tease apart any potential contributions of S2 to POm activity.

The Gain of CT Transfer Function Is Dynamic

Synaptic depression is a well-established feature of the L5B-POm pathway (Reichova and Sherman 2004; Groh et al. 2008). However, the consequences of synaptic depression on CT spike transfer in vivo were unknown. L5B spontaneous spiking rates of 3–4 Hz predict that the L5B-POm pathway is in a constant state of depression which prevents high gain CT spike transfer. However, the present in vivo data show that CT gain is not constant, but rather follows cortical Up and Down states, peaking at the transition point and declining sharply during the early phase of the Up

state. Large single EPSPs occur mostly during the beginning phase of the Up state (Figs 1 and 2), especially the very large EPSPs that are most likely associated with the T-type Ca2+ channel currents and bursting (Jahnsen and Llinas 1984; Seol and Kuner 2015). By evoking these "driver" EPSPs, isolated L5B spikes (i.e., spikes preceded by a Down state) have the highest chance to trigger one or more POm spikes; estimates from the intracellular data suggest that nearly half of APs are triggered by such "driver" EPSPs. Subsequently, as EPSP amplitudes decline during the Up state (Figs 2 and 7), 2 or more EPSPs must be integrated to trigger POm spiking; such integration can occur in single input neurons for EPSPs separated by short IEIs, or in multiple input neurons for near coincident EPSPs.

These data demonstrate that the L5B-POm pathway shows pronounced frequency-dependent adaptation in vivo, and it is likely that synaptic depression is a main contributing mechanism. A simple model based on a few experimentally derived rules could recreate the time course and essential features of the L5B-POm spike transfer (Fig. 7), showing that the dynamics of POm spiking during Up states is largely explained by EPSP adaptation driven by L5B spontaneous spiking. Even though in vivo adaptation does not reach the extremes measured in vitro (Groh et al. 2008), we find that EPSP adaptation has functional consequences for CT spike transfer and underlies the dynamic gain of this pathway.

Given the complex nonlinear properties of POm neurons (Landisman and Connors 2007) and the voltage and time dependence of thalamic intrinsic mechanisms such as the T-type calcium and HCN channels (Jahnsen and Llinas 1984; McCormick and Pape 1990; Sherman 2001), it is noteworthy that EPSP adaptation is ensured by multiple intrinsic mechanisms in combination with presynaptic depression. The amplitudes of temporally isolated "driver" EPSPs in particular were decreased by depolarization (see Supplementary Fig. 7*D*), consistent with the presence of a T-type calcium component. In agreement with recent in vitro T-type calcium knockdown findings (Seol and Kuner 2015), these data suggest that the T-type calcium current contributes significantly to thalamic excitability to specifically enhance isolated or low frequency events. Thus, the interplay between multiple pre- and postsynaptic mechanisms strongly suggests that adaptation is a key feature of the L5B-POm pathway.

Finally, it remains to be determined exactly how the in vivo EPSP adaptation we report here interacts with changes in membrane potential elicited by modulatory inputs, in particular from CT L6 pathways (Lam and Sherman 2010; Mease et al. 2014; Crandall et al. 2015) and subcortical inhibition (Veinante, Lavallee, et al. 2000; Bartho et al. 2002; Trageser and Keller 2004; Lavallee et al. 2005; Bartho et al. 2007).

Expected L5B-POm Spike Transfer in the Awake Animal

In the awake rat, L5B neurons spike at 3–4 Hz (de Kock and Sakmann 2008, 2009; Oberlaender et al. 2012), predicting that this pathway may predominantly operate as an integrator of inputs. However, even at intermediate gains expected at these rates, only a few simultaneous L5B inputs would be needed to elicit POm spikes. This is a very different situation compared with thalamocortical connections, in which many synchronous thalamic inputs are required to trigger cortical spiking (Gabernet et al. 2005; Bruno and Sakmann 2006; Jia et al. 2014). Furthermore, in the awake animal, cortical spiking occurs in structured patterns (Luczak et al. 2007) with periods of inactivity, suggesting that CT spike transfer may in principle occur with high gain in the awake state. It is likely that inputs from higher order cortical areas such as S2 (Liao et al. 2010) and deep layers of motor cortex (Hooks et al. 2013) contribute substantially to POm spiking in the awake animal. Furthermore, L6 CT neurons—which probably contributed very little to POm activity in this study, due to "ultrasparse" spontaneous firing rates of approximately 0.1 Hz (Velez-Fort et al. 2014)—likely play a more important role during wakefulness. While recent reports show that POm neurons are indeed quite active in the awake animal (Moore et al. 2015; Urbain et al. 2015) and produce relatively complex spikes trains with long and short interspike intervals, the relationship between cortical and POm spiking described here remains to be investigated under nonanesthetized conditions.

Possible Role of the L5B-POm Pathway in Transferring Cortical Spike Output Through CT Circuits

It has been suggested that the majority of brain activity reflects "internal states," that is, spiking activity that is independent of sensory input, and that sensory inputs serve to modulate or suspend this activity (Llinas and Pare 1991; Raichle et al. 2001; Kenet et al. 2003; Ringach 2009; Destexhe 2011). In human fMRI studies, Raichle and colleagues (Zhang et al. 2008) report strong correlations between the cortex and the thalamus during spontaneous oscillations associated with the "default network state" (Raichle et al. 2001) of the resting brain. Spread of such internal cortical state throughout the cortico-thalamo-cortical network may employ CT signaling via higher order thalamic nuclei.

The idea that higher order nuclei route cortical activity to other cortical areas was first formulated by Sherman and colleagues (Sherman and Guillery 1996, 2006; Reichova and Sherman 2004). Here we provide evidence that in vivo, the higher order nucleus POm is indeed strongly activated by cortical input from L5B, particularly isolated L5B spikes occurring after periods of silence. However, a direct measure of CT convergence, that is, count of the number of anatomical L5B inputs per POm neuron, has yet to be achieved. Here, as an indirect first estimate of CT convergence, we find that during Up/Down state oscillations, each POm neuron receives functional input from a low number of active L5B neurons. Estimates from 2 different methods suggest that under these experimental conditions, approximately one-third of the POm neurons have only one active L5B input, with an average of 2.5 L5B input neurons per POm neuron (Fig. 8). Thalamus-projecting L6 neurons are ultrasparse firing (Velez-Fort et al. 2014) and evoke small and slow EPSPs (Reichova and Sherman 2004; Landisman and Connors 2007), making it unlikely that L6 inputs contributed significantly to this convergence analysis. However, it should be noted that both the level of functional CT convergence and the contribution of L6 input are most likely dependent on behavioral state.

These results suggest that single or synchronized spikes of a few BC L5B neurons can be amplified at the CT driver synapse and "broadcast" via POm simultaneously to motor, primary, and secondary sensory cortical via the widespread projections POm makes to various cortical areas (Deschenes et al. 1998; Meyer et al. 2010; Theyel et al. 2010). Consistent with this amplification and broadcasting idea is the net excitatory effect of POm on cortical networks (Bureau et al. 2006; Petreanu et al. 2009; Theyel et al. 2010; Viaene et al. 2011; Gambino et al. 2014; Jouhanneau et al. 2014) to enhance and prolong cortical sensory responses (Mease et al. 2016).

Supplementary Material

Supplementary material can be found at http://www.cercor.oxfordjournals.org/.

Funding

This work was supported by the Deutsche Forschungsgemeinschaft Sachbeihilfe (GR 3757/1-1) (R.A.M), the Max Planck Society (A.G., A.S., B.S., R.A.M.), the Institute of Advanced Studies at the TU München (A.G.), and Boehringer Ingelheim Fonds (A.S.). Funding to pay the Open Access publication charges for this article was provided by the Max Planck Society.

Notes

We thank Arthur Konnerth for providing lab space, infrastructure and support at the Institute for Neuroscience at the TU München, and Christiaan de Kock, Patrik Krieger, Randy Bruno and Erwin Neher for comments on earlier versions of this manuscript. Thy-1-ChR2 mice were a gift from Karl Deisseroth. *Conflict of Interest*: None declared.

References

Arenkiel BR, Peca J, Davison IG, Feliciano C, Deisseroth K, Augustine GJ, Ehlers MD, Feng G. 2007. In vivo light-induced activation of neural circuitry in transgenic mice expressing channelrhodopsin-2. Neuron. 54:205–218.

Bartho P, Freund TF, Acsady L. 2002. Selective GABAergic innervation of thalamic nuclei from zona incerta. Eur J Neurosci. 16:999–1014.

Bartho P, Slezia A, Varga V, Bokor H, Pinault D, Buzsaki G, Acsady L. 2007. Cortical control of zona incerta. J Neurosci. 27:1670–1681.

Bourassa J, Pinault D, Deschenes M. 1995. Corticothalamic projections from the cortical barrel field to the somatosensory thalamus in rats: a single-fibre study using biocytin as an anterograde tracer. Eur J Neurosci. 7:19–30.

Bruno RM, Sakmann B. 2006. Cortex is driven by weak but synchronously active thalamocortical synapses. Science. 312:1622–1627.

Bureau I, von Saint Paul F, Svoboda K. 2006. Interdigitated paralemniscal and lemniscal pathways in the mouse barrel cortex. PLoS Biol. 4:e382.

Chiaia NL, Rhoades RW, Bennett-Clarke CA, Fish SE, Killackey HP. 1991. Thalamic processing of vibrissal information in the rat. I. Afferent input to the medial ventral posterior and posterior nuclei. J Comp Neurol. 314:201–216.

Constantinople CM, Bruno RM. 2011. Effects and mechanisms of wakefulness on local cortical networks. Neuron. 69:1061–1068.

Crandall SR, Cruikshank SJ, Connors BW. 2015. A corticothalamic switch: controlling the thalamus with dynamic synapses. Neuron. 86:768–782.

de Kock CP, Bruno RM, Spors H, Sakmann B. 2007. Layer- and cell-type-specific suprathreshold stimulus representation in rat primary somatosensory cortex. J Physiol. 581:139–154.

de Kock CP, Sakmann B. 2008. High frequency action potential bursts (>or=100 Hz) in L2/3 and L5B thick tufted neurons in anaesthetized and awake rat primary somatosensory cortex. J Physiol. 586:3353–3364.

de Kock CP, Sakmann B. 2009. Spiking in primary somatosensory cortex during natural whisking in awake head-restrained rats is cell-type specific. Proc Natl Acad Sci USA. 106:16446–16450.

Deschenes M, Timofeeva E, Lavallee P. 2003. The relay of high-frequency sensory signals in the Whisker-to-barreloid pathway. J Neurosci. 23:6778–6787.

Deschenes M, Veinante P, Zhang ZW. 1998. The organization of corticothalamic projections: reciprocity versus parity. Brain Res Rev. 28:286–308.

Destexhe A. 2011. Intracellular and computational evidence for a dominant role of internal network activity in cortical computations. Curr Opin Neurobiol. 21:717–725.

Diamond ME, Armstrong-James M, Budway MJ, Ebner FF. 1992. Somatic sensory responses in the rostral sector of the posterior group (POm) and in the ventral posterior medial nucleus (VPM) of the rat thalamus: dependence on the barrel field cortex. J Comp Neurol. 319:66–84.

Efron B, Tibshirani R. 1991. Statistical data analysis in the computer age. Science. 253:390–395.

Furuta T, Urbain N, Kaneko T, Deschenes M. 2010. Corticofugal control of vibrissa-sensitive neurons in the interpolaris nucleus of the trigeminal complex. J Neurosci. 30:1832–1838.

Gabernet L, Jadhav SP, Feldman DE, Carandini M, Scanziani M. 2005. Somatosensory integration controlled by dynamic thalamocortical feed-forward inhibition. Neuron. 48:315–327.

Gambino F, Pages S, Kehayas V, Baptista D, Tatti R, Carleton A, Holtmaat A. 2014. Sensory-evoked LTP driven by dendritic plateau potentials in vivo. Nature. 515:116–119.

Groh A, Bokor H, Mease RA, Plattner VM, Hangya B, Stroh A, Deschenes M, Acsady L. 2014. Convergence of cortical and sensory driver inputs on single thalamocortical cells. Cereb Cortex. 24:3167–3179.

Groh A, de Kock CP, Wimmer VC, Sakmann B, Kuner T. 2008. Driver or coincidence detector: modal switch of a corticothalamic giant synapse controlled by spontaneous activity and short-term depression. J Neurosci. 28:9652–9663.

Groh A, Krieger P. 2011. Structure–function analysis of genetically defined neuronal populations. In: Fritjof H, Arthur K, Yuste R, editors. Imaging in neuroscience: a laboratory manual. Cold Spring Harbor: Cold Spring Harbor Laboratory Press.

Hahn TT, Sakmann B, Mehta MR. 2006. Phase-locking of hippocampal interneurons' membrane potential to neocortical up-down states. Nat Neurosci. 9:1359–1361.

Hoogland PV, Welker E, Van der Loos H. 1987. Organization of the projections from barrel cortex to thalamus in mice studied with Phaseolus vulgaris-leucoagglutinin and HRP. Exp Brain Res. 68:73–87.

Hoogland PV, Wouterlood FG, Welker E, Van der Loos H. 1991. Ultrastructure of giant and small thalamic terminals of cortical origin: a study of the projections from the barrel cortex in mice using Phaseolus vulgaris leuco-agglutinin (PHA-L). Exp Brain Res. 87:159–172.

Hooks BM, Mao T, Gutnisky DA, Yamawaki N, Svoboda K, Shepherd GM. 2013. Organization of cortical and thalamic input to pyramidal neurons in mouse motor cortex. J Neurosci. 33:748–760.

Jahnsen H, Llinas R. 1984. Ionic basis for the electro-responsiveness and oscillatory properties of guinea-pig thalamic neurones in vitro. J Physiol. 349:227–247.

Jia H, Varga Z, Sakmann B, Konnerth A. 2014. Linear integration of spine Ca2+ signals in layer 4 cortical neurons in vivo. Proc Natl Acad Sci USA. 111:9277–9282.

Jouhanneau JS, Ferrarese L, Estebanez L, Audette NJ, Brecht M, Barth AL, Poulet JF. 2014. Cortical fosGFP expression reveals broad receptive field excitatory neurons targeted by POm. Neuron. 84:1065–1078.

Kelly MK, Carvell GE, Hartings JA, Simons DJ. 2001. Axonal conduction properties of antidromically identified neurons in rat barrel cortex. Somatosens Mot Res. 18:202–210.

Kenet T, Bibitchkov D, Tsodyks M, Grinvald A, Arieli A. 2003. Spontaneously emerging cortical representations of visual attributes. Nature. 425:954–956.

Killackey HP, Sherman SM. 2003. Corticothalamic projections from the rat primary somatosensory cortex. J Neurosci. 23:7381–7384.

Lam YW, Sherman SM. 2010. Functional organization of the somatosensory cortical layer 6 feedback to the thalamus. Cereb Cortex. 20:13–24.

Landisman CE, Connors BW. 2007. VPM and PoM nuclei of the rat somatosensory thalamus: intrinsic neuronal properties and corticothalamic feedback. Cereb Cortex. 17:2853–2865.

Lavallee P, Urbain N, Dufresne C, Bokor H, Acsady L, Deschenes M. 2005. Feedforward inhibitory control of sensory information in higher-order thalamic nuclei. J Neurosci. 25:7489–7498.

Letzkus JJ, Wolff SB, Meyer EM, Tovote P, Courtin J, Herry C, Luthi A. 2011. A disinhibitory microcircuit for associative fear learning in the auditory cortex. Nature. 480:331–335.

Li J, Guido W, Bickford ME. 2003. Two distinct types of corticothalamic EPSPs and their contribution to short-term synaptic plasticity. J Neurophysiol. 90:3429–3440.

Liao CC, Chen RF, Lai WS, Lin RC, Yen CT. 2010. Distribution of large terminal inputs from the primary and secondary somatosensory cortices to the dorsal thalamus in the rodent. J Comp Neurol. 518:2592–2611.

Llinas RR, Pare D. 1991. Of dreaming and wakefulness. Neuroscience. 44:521–535.

Luczak A, Bartho P, Marguet SL, Buzsaki G, Harris KD. 2007. Sequential structure of neocortical spontaneous activity in vivo. Proc Natl Acad Sci USA. 104:347–352.

Margrie TW, Brecht M, Sakmann B. 2002. In vivo, low-resistance, whole-cell recordings from neurons in the anaesthetized and awake mammalian brain. Pflugers Arch. 444:491–498.

McCormick DA, Pape HC. 1990. Properties of a hyperpolarization-activated cation current and its role in rhythmic oscillation in thalamic relay neurones. J Physiol. 431:291–318.

Mease RA, Krieger P, Groh A. 2014. Cortical control of adaptation and sensory relay mode in the thalamus. Proc Natl Acad Sci USA. 111:6798–6803.

Mease RA, Metz M, Groh A. 2016. Cortical sensory responses are enhanced by the higher-order thalamus. Cell Rep. 14:208–215.

Meyer HS, Wimmer VC, Hemberger M, Bruno RM, de Kock CP, Frick A, Sakmann B, Helmstaedter M. 2010. Cell type-specific thalamic innervation in a column of rat vibrissal cortex. Cereb Cortex. 20:2287–2303.

Moore JD, Mercer Lindsay N, Deschenes M, Kleinfeld D. 2015. Vibrissa self-motion and touch are reliably encoded along the same somatosensory pathway from brainstem through thalamus. PLoS Biol. 13:e1002253.

Oberlaender M, de Kock CP, Bruno RM, Ramirez A, Meyer HS, Dercksen VJ, Helmstaedter M, Sakmann B. 2012. Cell type-specific three-dimensional structure of thalamocortical circuits in a column of rat vibrissal cortex. Cereb Cortex. 22:2375–2391.

Paxinos G. 2001. The mouse brain in stereotaxic coordinates/George Paxinos, Keith B.J. Franklin. San Diego, (CA): Academic Press.

Petreanu L, Mao T, Sternson SM, Svoboda K. 2009. The subcellular organization of neocortical excitatory connections. Nature. 457:1142–1145.

Pinault D. 1996. A novel single-cell staining procedure performed in vivo under electrophysiological control: morpho-functional features of juxtacellularly labeled thalamic cells and other central neurons with biocytin or Neurobiotin. J Neurosci Methods. 65:113–136.

Poulet JF, Petersen CC. 2008. Internal brain state regulates membrane potential synchrony in barrel cortex of behaving mice. Nature. 454:881–885.

Raichle ME, MacLeod AM, Snyder AZ, Powers WJ, Gusnard DA, Shulman GL. 2001. A default mode of brain function. Proc Natl Acad Sci USA. 98:676–682.

Reichova I, Sherman SM. 2004. Somatosensory corticothalamic projections: distinguishing drivers from modulators. J Neurophysiol. 92:2185–2197.

Reimer J, Froudarakis E, Cadwell CR, Yatsenko D, Denfield GH, Tolias AS. 2014. Pupil fluctuations track fast switching of cortical states during quiet wakefulness. Neuron. 84:355–362.

Ringach DL. 2009. Spontaneous and driven cortical activity: implications for computation. Curr Opin Neurobiol. 19:439–444.

Seol M, Kuner T. 2015. Ionotropic glutamate receptor GluA4 and T-type calcium channel Ca 3.1 subunits control key aspects of synaptic transmission at the mouse L5B-POm giant synapse. Eur J Neurosci. 42:3033–3044.

Sherman SM. 2001. Tonic and burst firing: dual modes of thalamocortical relay. Trends Neurosci. 24:122–126.

Sherman SM, Guillery R. 2006. Exploring the thalamus and its role in cortical function. Cambridge (MA): MIT Press.

Sherman SM, Guillery RW. 1996. Functional organization of thalamocortical relays. J Neurophysiol. 76:1367–1395.

Slezia A, Hangya B, Ulbert I, Acsady L. 2011. Phase advancement and nucleus-specific timing of thalamocortical activity during slow cortical oscillation. J Neurosci. 31:607–617.

Steriade M. 1997. Synchronized activities of coupled oscillators in the cerebral cortex and thalamus at different levels of vigilance. Cereb Cortex. 7:583–604.

Stroh A, Adelsberger H, Groh A, Ruhlmann C, Fischer S, Schierloh A, Deisseroth K, Konnerth A. 2013. Making waves: initiation and propagation of corticothalamic ca(2+) waves in vivo. Neuron. 77:1136–1150.

Theyel BB, Llano DA, Sherman SM. 2010. The corticothalamocortical circuit drives higher-order cortex in the mouse. Nat Neurosci. 13:84–88.

Timofeev I, Contreras D, Steriade M. 1996. Synaptic responsiveness of cortical and thalamic neurones during various phases of slow sleep oscillation in cat. J Physiol. 494(Pt 1):265–278.

Trageser JC, Keller A. 2004. Reducing the uncertainty: gating of peripheral inputs by zona incerta. J Neurosci. 24:8911–8915.

Urbain N, Salin PA, Libourel PA, Comte JC, Gentet LJ, Petersen CC. 2015. Whisking-related changes in neuronal firing and membrane potential dynamics in the somatosensory thalamus of awake mice. Cell Rep. 13:647–656.

Vazquez AL, Fukuda M, Crowley JC, Kim SG. 2014. Neural and hemodynamic responses elicited by forelimb- and photostimulation in channelrhodopsin-2 mice: insights into the hemodynamic point spread function. Cereb Cortex. 24:2908–2919.

Veinante P, Jacquin MF, Deschenes M. 2000. Thalamic projections from the whisker-sensitive regions of the spinal trigeminal complex in the rat. J Comp Neurol. 420:233–243.

Veinante P, Lavallee P, Deschenes M. 2000. Corticothalamic projections from layer 5 of the vibrissal barrel cortex in the rat. J Comp Neurol. 424:197–204.

Velez-Fort M, Rousseau CV, Niedworok CJ, Wickersham IR, Rancz EA, Brown AP, Strom M, Margrie TW. 2014. The stimulus selectivity and connectivity of layer six principal cells reveals cortical microcircuits underlying visual processing. Neuron. 83:1431–1443.

Viaene AN, Petrof I, Sherman SM. 2011. Properties of the thalamic projection from the posterior medial nucleus to primary and secondary somatosensory cortices in the mouse. Proc Natl Acad Sci USA. 108:18156–18161.

Vyazovskiy VV, Olcese U, Hanlon EC, Nir Y, Cirelli C, Tononi G. 2011. Local sleep in awake rats. Nature. 472:443–447.

Wimmer VC, Nevian T, Kuner T. 2004. Targeted in vivo expression of proteins in the calyx of Held. Pflugers Arch. 449:319–333.

Xu NL, Harnett MT, Williams SR, Huber D, O'Connor DH, Svoboda K, Magee JC. 2012. Nonlinear dendritic integration of sensory and motor input during an active sensing task. Nature. 492:247–251.

Zhang D, Snyder AZ, Fox MD, Sansbury MW, Shimony JS, Raichle ME. 2008. Intrinsic functional relations between human cerebral cortex and thalamus. J Neurophysiol. 100:1740–1748.

Zhao S, Ting JT, Atallah HE, Qiu L, Tan J, Gloss B, Augustine GJ, Deisseroth K, Luo M, Graybiel AM, et al. 2011. Cell type-specific channelrhodopsin-2 transgenic mice for optogenetic dissection of neural circuitry function. Nat Methods. 8: 745–752.